論文

Electro-Micromechanical 시험법과 Acoustic Emission을 이용한 단섬유/시멘트 복합재료의 미세파괴 메커니즘과 비파괴적 평가

박종만*+, 이상일*, 김진원*, 윤동진**

Nondestructive Evaluation and Microfailure Mechanisms of Single Fibers/Brittle Cement Matrix Composites using Electro-Micromechanical Technique and Acoustic Emission

J. M. Park*+, S. I. Lee*, J. W. Kim*, D. J. Yoon**

ABSTRACT

Interfacial and microfailure properties of the modified steel, carbon and glass fibers/cement composites were investigated using electro-pullout test under tensile and compressive tests with acoustic emission (AE). The hand-sanded steel composite exhibited higher interfacial shear strength (IFSS) than the untreated and even neoalkoxy zirconate (Zr) treated steel fiber composites. This might be due to the enhanced mechanical interlocking, compared to possible hydrogen or covalent bonds. During curing process, the contact resistivity decreased rapidly at the initial stage and then showed a level-off. Comparing to the untreated case, the contact resistivity of either Zr-treated or hand-sanded steel fiber composites increased to the infinity at latter stage. The number of AE signals of hand-sanded steel fiber composite was much more than those of the untreated and Zr-treated cases due to many interlayer failure signals. AE waveforms for pullout and frictional signals of the hand-sanded composite are larger than those of the untreated case. For dual matrix composite (DMC), AE energy and waveform under compressive loading were much higher and larger than those under tensile loading, due to brittle but well-enduring ceramic nature against compressive stress. Vertical multicrack exhibits for glass fiber composite under tensile test, whereas buckling failure appeared under compressive loading. Electro-micromechanical technique with AE can be used as an efficient nondestructive (NDT) method to evaluate the interfacial and microfailure mechanisms for conductive fibers/brittle and nontransparent cement composites.

초 록

인장 및 압축 하중하에서 electro-pullout 시험법과 음향방출법을 이용하여, 표면 처리된 steel fiber, 탄소 그리고 유리 섬유/시멘트복합재료의 계면 물성과 미세파괴구조를 평가하였다. 기계적 interlocking을 증가시킨 steel fiber 복합재료의 계면전단강도가 미처리 또는 neoalkoxy zirconate (Zr) 처리된 steel fiber 복합재료보다 더 향상되었음을 보여주었다.

*+ 경상대학교 응용화학공학부/고분자공학전공, 항공기부품기술연구센터, 교신저자(E-mail:jmpark@nongae.gsnu.ac.kr)
* 경상대학교 응용화학공학부/고분자공학전공, 항공기부품기술연구센터
** 한국표준과학연구원 비파괴평가그룹

이것은 존재 가능한 수소결합 또는 공유결합에 비해 기계적 interlocking이 계면 물성에 더 많은 영향을 주기 때문으로 고찰된다. 시멘트복합재료를 경화하는 동안에, 접촉 저항도는 초기에는 급격히 감소하였으나, 이후 증가치가 둔화되는 현상을 보였다. Zr처리 및 기계적 interlocking을 향상시킨 steel fiber 복합재료의 접촉저항은 미처리의 경우에 비해 더 나중 단계에서 무한대로 증가하였다. 기계적 interlocking이 향상된 steel fiber 복합재료의 계면 파괴에 의한 음향방출 신호의 수가 미처리 또는 Zr 처리된 복합재료에 비해 훨씬 많이 나타났다. 기계적 맞물림이 향상된 복합재료의 pullout과 마찰신호에 대한 음향방출 파형이 미처리에 비해 크게 나타났다. Dual matrix composite (DMC)에서, 압축하중 하에서의 음향방출 에너지와 파형이 인장하중 하에서의 에너지와 파형에 비해 더 크게 나타났는데, 이것은 시멘트 복합재료가 압축응력을 잘 견디는 세라믹 성질에 기인한 것으로 고찰된다. 유리섬유 복합재료의 인장 시험에서는 수직균열이 나타났고, 반면에 압축 시험에서는 buckling 균열현상이 관찰되었다. Electro-micromechanical시험법과 음향방출법은 전도성 섬유가 보강된 불투명한 취성기지 복합재료의 계면 물성과 미세 파괴구조를 평가하기위한 효율적인 비파괴시험법으로 사용될 수 있다.

1. INTRODUCTION

Microfailure mechanisms of cement matrix composite (CMC) are basically different from polymer matrix composite (PMC). The characteristic properties of a brittle ceramic matrix are generally low tensile strength and strain to failure, whereas compressive strength can exhibit very high. The toughness of fiber reinforced brittle-ceramic matrix composite is much higher than brittle monolithic matrix materials [1,2]. The fracture toughness of CMC can be provided by fiber bridging mechanism in the ceramic matrix cracks. Too strong interfacial bonding does not desire in a CMC, because it would make a crack run through the specimen, whereas a suitably strong interface would lead to fiber bridging by matrix microcracks. A CMC with even many microcracked matrix can retain some reasonable strength. The main disadvantage is that matrix microcracking provides an easy path for environment attack of the fibers and the fiber/matrix interface.

Curtin [3-5] proposed various theories and models for matrix crack mechanism and the interfacial dependence of CMC based on micromechanical theorems. Many matrix cracks (or called as multiple matrix cracks) are generated prior to the catastrophic failure of the composite. Singh [6] studied the first-matrix cracking stress and IFSS in SiC fiber/zircon matrix composites with either the untreated or BN-coated. The first matrix cracking stress was measured by either tension or flexure, whereas IFSS was measured by fiber pushout test. The first matrix cracking stress was independent upon the measured IFSS, but showed a good correlation with the first matrix strain.

Single fiber pullout test [7,8] is a well-known method to investigate IFSS because it can measure directly interfacial adhesion, and it is not limited by the properties of the fiber and matrix. In fragmentation test [9-11], the failure elongation of the matrix should be several times larger than the failure elongation to cause a saturated fragmentation state. This method is not adequate for less brittle fiber/brittle matrix composite system. DMC specimen [12,13] is basically modified from the single fiber composite (SFC) test. DMC specimen is composed of a single fiber, a brittle layer (inner matrix for measuring IFSS) and ductile matrix (supportable outer matrix). The specimen was subjected to tensile loading and resulted in many fragments of the embedded fiber and the brittle coating layer. Park [14] studied interfacial properties and microfailure mechanisms of DMC of single glass fiber/brittle unsaturated polyester/ductile epoxy using micromechanical technique and AE.

Single fiber Broutman test [15,16] was recently used to investigate interfacial properties and microfailure mechanism by subjecting to compressive load. This technique was performed to apply a transverse stress to the interface in a single necked specimen. Under compressive load, the interfacial debonding and buckling behaviors were investigated with an aid of AE. Wood *et al.* [17-19] studied the compressive fragmentation test, i.e. single fiber Broutman test, to evaluate single fiber compressive strength, Weibull parameters, thermal stress and IFSS.

AE is known as one of the important NDT methods [20,21]. The AE can monitor the fracture behavior of composite materials, and can characterize many AE parameters to understand the type of microfailure sources

during the fracture progressing. When tensile loading is applied to a composite, AE signal may occur from fiber fracture, matrix cracking, and debonding at the fiber/matrix interface. AE energy released by the fiber fracture can be greater than that associated by debonding or matrix cracking. Park [22,23] studied interfacial properties and microfailure mechanism of the untreated and electrodeposited fibers/epoxy composites using AE as well as the fragmentation test. Three distinct AE signals were observed from fiber, interlayer and matrix in microcomposite specimens. More AE events occurred due to interlayer failure in the treated composite.

Recently, many researchers [24-29] had been trying to evaluate composite characteristics by a measurement of electrical and micromechanical properties. Yuse [24] used the electrical resistance measurement as a smart NDT testing method. The relationship between electrical resistance and fiber breakage/delamination in carbon fiber reinforced plastics (CFRP) laminate was studied by tensile and fatigue tests. Especially, single fiber electro-pullout test was reported initially by Chung *et al.* [25-28]. To provide the information on the interfacial adhesion and microfailure modes, the contact resistivity of carbon or steel fiber/cement matrix composites was measured. The contact resistivity was correlated to interfacial adhesion as a function of fiber surface treatment and mixing ratio of cement paste/water. A new evaluation of interfacial properties including the measurement of curing characteristics through the electrical resistivity measurement were also investigated in carbon fiber reinforced epoxy composites [29].

In this work, electro-micromechanical technique with AE was used to evaluate interfacial characteristics and microfailure modes of the treated fiber reinforced brittle cement composites compared to the untreated case. The fracture mechanisms coming from the interface and brittle ceramic matrix were correlated with the contact and the electrical resistivity and AE events depending on the fiber surface treatments.

2. EXPERIMENTAL

2.1 Materials

Carbon fiber with diameter of 18 ㎛ (Mitsubishi Chemical Co., Japan) and steel fiber with diameter of 280 ㎛ were used for single fiber electro-pullout test, and glass fiber with diameter of 125 ㎛ was used for tensile/compressive DMC test. Table 1 shows the electrical properties of bare conductive fibers and cement composites. Early strength Portland cement (Type Ⅲ, Ssangyong Cement Industrial Co., Korea) was used as an inner brittle matrix. For preparing DMC specimen, an outer matrix was made of the mixture of epoxy resin (YD-128, Kukdo Chemical Co., Korea) based on diglycidyl ether of bisphenol-A (DGEBA) and polyoxypropylene diamine curing agents (Jeffamine D-400 and D-2000, Huntzman Petrochemicals Co.). Matrix modulus was adjusted properly by relative mixing proportion of D-400 *versus* D-2000 to obtain the optimum ductility for electro-micromechanical testing. Neoalkoxy zirconate (NJ-38J, Kenrich Petrochemicals Inc.) for fiber surface treatment was used as a coupling agent. The chemical structure of neoalkoxy zirconate (Zr) coupling agent is

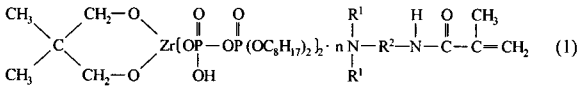

(1)

where R is alkyl group, and n is constant, respectively.

2.2 Methodologies

2.2.1 Fiber Surface Treatments and Testing Specimen Preparation

Twenty untreated steel, carbon and glass fibers were fixed with suitable distance apart in each rectangular frame. The salt of Zr coupling agent was diluted to 7 wt% concentration with ethanol. Three different fibers were dipped into Zr coupling agent in ethanol solution for 2 minutes. After dip-coating process, all fibers were dried for 2 hours at room temperature without further thermal treatment. Some steel fibers were treated by hand-sanded way with very fine sand paper (#400) to enhance the mechanical interlocking effect.

Figure 1 shows three testing specimens for (a) electro-pullout test specimen whereas (b) tensile and (c) compressive specimens for micromechanical tests. For electro-pullout specimen, the untreated and the treated steel or carbon fibers were fixed in the silicone mold, and then

cement paste filled into the mold. Cement paste was made of Portland cement and deionized water with the weight ratio of 100:30, and then was mixed by a mechanical stirrer rod for 10 minutes. Single fiber cement composite was cured at 25 ℃, 90 % humidity for 3 days. After curing process, two pairs of copper wire were laid down on the position of two voltages and contact probes in the microspecimen. The intersecting point between copper wire and specimen was connected electrically with a silver paste. To avoid electrical contact between the microspecimen and the jig of the universal testing machine (UTM), the exposed surface of cement matrix was coated by an epoxy adhesive. In DMC, cement was acted as an inner matrix, whereas epoxy resin was acted as an outer matrix. Single glass fiber was fixed at the frame, and then cement paste was coated on the fiber. After curing process immediately, glass fiber/thin cement composite was fixed in the silicone mold. After epoxy mixture was poured into the mold, epoxy was precured at 80 ℃ for 2 hours and then postcured at 120℃ for 2 hours. Surface topography of steel and carbon fibers were observed by scanning electron microscope (SEM, Model JSM6400, JOEL Co.) The fibers were coated with gold sputtering for 30 seconds before observation, and working distance in SEM was 18 mm.

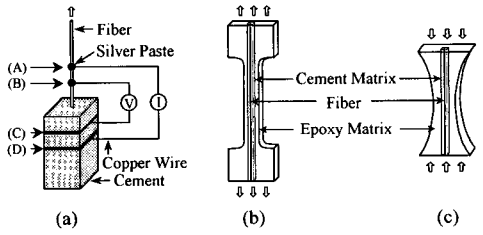

Fig. 1 Three testing specimens for (a) electro-pullout test specimen; and (b) tensile and (c) compressive spec -imens for micromechanical tests.

2.2.2 Measurements of IFSS and Microfailure Modes

In single fiber electro-pullout test, tensile load was applied in UTM with attached load cell of 10 KN for steel fiber composite and 100 N for carbon fiber composite, respectively. Crosshead speed was 0.5 mm/minute for both cases. After the electro-pullout specimen was fixed in the jig, the specimen was strained incrementally and tensile load was applied until the fiber was pulled out from cement matrix. The shear force developed at the interface between conductive fiber and matrix was measured during electro-pullout testing. IFSS of microspecimen can be derived from the maximum pullout force, F_d as

$$\tau_i = \frac{F_d}{\pi \ D_f L} \tag{2}$$

where D_f and L are fiber diameter and fiber embedded length in the cement, respectively.

To obtain IFSS and microfailure modes, tensile and compressive tests for DMC specimen were carried out using UTM with load cell of 10 KN and strain rate of 0.5 mm/minute. Ultimate brittle matrix cracking and subsequent failure process were observed and measured under a polarized-light microscope. When a DMC specimen is stressed tensilely to the fiber axis, multiple fracture of brittle cement matrix can occur, and the fiber can endure the applied stress when the matrix fails. The relationship between IFSS, and matrix crack spacing, x is given by the following equation [14],

$$x = \frac{V_m \sigma_{mu} d}{2 V_f \tau} \tag{3}$$

where V_m and V_f are the volume fraction of the matrix and fiber, respectively, d is the fiber diameter and mu is the stress at which the crack begins to form.

2.2.3 Measurements of Electrical and Contact Resistivity

The electrical resistivity of various conductive bare fibers and the contact resistivity of single fiber/cement composite were measured using a HP34401A digital multimeter. The well-known four-probe method [25] was used for measuring the electrical resistance between two voltage probes (junction B and C). Silver paste was used as an electrically connecting glue at junctions A, B, C and D for the electrical contact between the microspecimen and leading wire during curing process and the electro-pullout testing. The electrical resistivity of the bare steel or carbon fiber was measured at

32 mm in the distance between two voltage contacts, whereas the contact resistivity of the fiber reinforced cement composites was monitored at 10 mm in the distance between two voltage contacts. The electrical resistivity of a bare fiber was obtained from the measured electrical resistance, the cross-sectional area of the conductive fiber, A and electrical contact length, L_{ec} between voltage contacts. The relationship between the electrical resistivity, ρ and resistance, R is

$$\rho = \left(\frac{A}{L_{ec}}\right) \times R \tag{4}$$

Total electrical resistance, R_{tot} between B and C may include R_s based on the contact resistance by silver paste plus R_f due to the resistance by fiber as

$$R_{tot} = R_s + R_f \tag{5}$$

Since the value of R_s is negligibly small due to very high conductivity of silver paste comparing to R_f, it can be considered that the voltage developed between junction B and C reflects nearly the fiber resistance,

$$R_{tot} = R_s + R_f \tag{6}$$

The contact resistivity of conductive fiber/cement composite can be different from that for the electrical resistivity of a bare fiber. Contact resistance, R_c and volume resistance, R_v are related to the contact resistivity, ρ_c and volume resistivity, ρ_v, respectively.

$$R_c = \frac{\rho_c}{A_c} \tag{7}$$

$$R_v = \rho_v \frac{l}{A_v} \tag{8}$$

Where A_c and l are the contact area and the length of the conductive fibers, respectively. The total measured resistance, R_T between the voltage probes is as follows:

$$R_T = R_v^{fiber} + R_c + R_v^{matrix} \tag{9}$$

Since conductivity of fibers is very high, R_v^{fiber} is negligible. By choosing a matrix that is small in dimension in the plane perpendicular to the fiber and choosing a matrix that is not too high in volume resistivity, R_v^{matrix} is negligible, so that equation (9) becomes

$$R_T = R_c \tag{10}$$

Once R_c is determined, ρ_c can be obtained from equation (7). The quantity ρ_c does not depend on the geometry but depends only on the structure or the property of the interface. Since it is nondestructive, the measurement of ρ_c does not require any pullout of the fiber. However, the measurement of ρ_c during fiber pullout testing can give further valuable information on the interface [25]. The contact resistivity of conductive fiber/cement composite was measured during curing process for 3 days. After the specimen was fixed at the UTM, the composite and the multimeter were connected electrically using leading wires. While the tensile load was applied continuously, the contact resistance of the specimen was monitored simultaneously.

2.2.4 AE Measurement

Microspecimen was mounted on the UTM to apply unidirectional tensile or compressive load. AE sensor was attached on the center of the specimen using a vacuum couplant. While AE signals were monitored during testing, microfailure modes of specimen were observed. During electro-pullout testing, AE signal was detected by a miniature sensor (Resonance type, Model PICO, Physical Acoustic Co.) with peak sensitivity of -68 Ref. V/m bar and resonant frequency at 550 kHz. The sensor output was amplified by 40 dB at preamplifier and passed through a band-pass filter was a range of 220 kHz to 750 kHz. For tensile and compressive tests, AE signal was detected using a wide band sensor (Broadband type mode, WD by PAC) with peak sensitivity of -62.5 Ref V/mbar and resonant frequency at 650 kHz.

The sensor output was amplified by 40 dB at preamplifier and passed through a band-pass filter with a range of 100 kHz to 1000 kHz. The signal was fed into AE processing unit (MISTRAS 2001 system) and then AE parameters were analyzed. Typical AE parameters such as hit rate, peak

amplitude and event energy were investigated in terms of testing time and distribution analysis. In order to obtain characteristic frequencies, AE waveform was analyzed by in built program for fast *Fourier* transform (FFT).

3. RESULTS AND DISCUSSION

3.1 IFSS, Contact Resistivity and AE Analysis by Single Fiber Electro-Pullout Test

Table 1 shows electrical properties of conductive bare fibers and fiber/cement composites depending on the fiber surface treatments at the initial stage. Both the electrical and the contact resistivity of carbon fiber composites were larger than those of steel fiber composites due to higher electrical resistivity of carbon fiber compared to steel fiber. The electrical and the contact resistivity of the treated case increased comparing to both the untreated steel and carbon fiber composites. This might be because of the insulating layer formed by Zr coupling agent on the fiber surface. Especially, the contact resistivity was the highest in the hand-sanded case. It might be due to the micro-void that could act as an electrical insulator based on the insufficient wetting between the fiber and cement.

Figure 2 showed the contact resistivity with the elapsed time in the untreated steel or carbon fiber composites during curing process. In both cases, the contact resistivity decreased abruptly at the initial stage, and then showed a level-off at the latter stage. The contact resistivity was actually measured after 1 day passed because it is very difficult to measure directly the contact resistivity at the initial state of the cement paste. Solid line is the measured data, whereas dot line is the expecting data.

Table 2 shows IFSS and the maximum load of steel or carbon fiber composites with the surface treatment by electro-pullout test. IFSS of the hand-sanded specimen was higher than both the untreated and Zr-treated cases, whereas that of the untreated specimen was the lowest. It might be considered that the mechanical interlocking was more effective than that of chemical coupling agent. Comparing to the untreated steel fiber composite, IFSS of the untreated carbon fiber composite was significantly lower. It might be considered that the interfacial compatibility between steel fiber

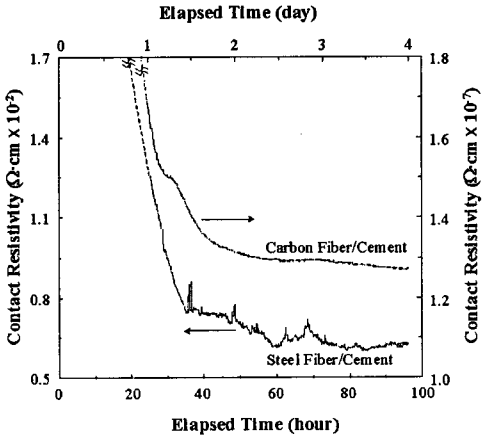

Fig. 2 The contact resistivity behavior for the untreated steel or carbon fiber/cement composites with the elapsed time.

and cement was much better than that between carbon fiber and cement. It can be considered that chemical reactions between fiber and Zr coupling agent, and between coupling agent and cement matrix could be possible for steel and carbon fiber composites. There could be hydrogen and covalent bonding at two each interface. The bonding might contribute to the effective IFSS and the occurrence of many AE events coming from the interfacial microfailure.

Figure 3 shows the contact resistivity, AE energy, shear stress of steel fiber composite depending on the surface treatment by the electro-pullout test and AE. The contact resistivity of (a) the untreated steel fiber composite increased suddenly at the initial stage, whereas those of (b) Zr-treated and (c) hand-sanded fiber composites increase at the latter stage. Although the fiber pullout occurred in Zr-treated and hand-sanded composites, the contact resistivity did not increase to the infinity at the maximum pullout strength as the untreated case. It could be considered that the interface was kept on contacting electrically, and thus maintaining the partial electrical contact until the strain applied further. The number of AE signals of the hand-sanded steel fiber composite was much more than that of the untreated and Zr-treated cases.

The maximum pullout strength of the hand-sanded case was larger than that of the untreated and Zr-treated composites. From stress *versus* strain curve, the fracture toughness of hand-sanded case was the largest than those of the untreated

Table 1 Resistivity properties of the steel and carbon fiber/cement composites at the initial stage

Fiber	Surface Condition	Diameter (μm)	Electrical Resistance (Ω)	Electrical Resistivity ($\Omega \cdot$ cm) $\times 10^{-4}$	Contact Resistance (Ω)	Contact Resistivity ($\Omega \cdot cm^2$)
Steel	Untreated	280	0.57 (0.07)*	1.09 (0.14)	670.4 (19.4)	76.2 (2.2)
	Hand-sanded[1)]	272	0.59 (0.10)	1.10 (0.19)	1127.7 (53.7)	128.2 (6.1)
	Zr-Treated[2)]	279	0.62 (0.05)	1.16 (0.10)	740.4 (41.2)	84.2 (4.8)
Carbon	Untreated	18	1.57×10^3 (120)	12.5 (1.0)	650.1×10^3 (75.7×10^3)	12.9×10^6 (1.51×10^3)
	Zr-Treated	18	1.64×10^3 (224)	12.9 (1.8)	658.2×10^3 (89.2×10^3)	13.1×10^6 (1.77×10^3)

* Parenthesis is standard deviation.
* Electrical resistance of steel and carbon fibers was measured at gauge length in 32 mm.
* Contact resistance of steel and carbon fiber/cement composites was at gauge length in 10 mm.
1) Hand-sanded with sand paper of #400
2) Treated by 7 wt% Zr-containing coupling agent ethanol solution

Table 2 IFSS and the maximum load of steel and carbon fiber cement composites depending on the surface treatment using single fiber electro-pullout test

Fiber	Surface Condition	Diameter (μm)	Maximum Load (Kgf)	IFSS[1)] (MPa)
Steel	Untreated	280	9.2 (0.3)*	10.3 (0.3)
	Hand-sanded	272	14.1 (0.6)	15.7 (0.7)
	Zr-treated	279	11.3 (0.4)	12.5(0.5)
Carbon	Untreated	18	0.051 (0.004)	4.43 (0.1)
	Zr-treated	18	0.047 (0.005)	4.12 (0.1)

* Parenthesis is standard deviation.
1) IFSS was calculated using equation (2).

or even Zr-treated cases due to the difference in energy absorption amount at the interface.

Figure 4 shows the changes of the contact resistivity and shear strength of (a) the untreated and (b) Zr-treated carbon fiber composite depending on the displacement and total testing time. This figure showed the trend of the whole range during the electro-pullout testing. For the untreated case, the contact resistivity increased steadily until it reached to the infinity, whereas the stress since the maximum decreased gently to the zero until the fiber was pulled out. On the other hand, for the Zr-treated case, the contact resistivity increased more likely stepwise than the untreated case, whereas the stress after the maximum decreased also stepwise and then showed a steady state, and finally dropped to zero. After the carbon fiber started to pull out for both cases, there might be the increased electrical disconnection by the interfacial failure. Finally, the contact resistivity of carbon fiber composite increased to the infinity at the complete electrical disconnection. The maximum load and shear strength for both cases were similar to each other. This might be considered that Zr coupling agent did not contribute to the interfacial bonding as expected. However, severer frictional resistance during pulling out is important to the performance of the CMC.

Figure 5 shows the changes of the logarithmic contact resistivity and shear strength of (a) the untreated and (b) Zr-treated carbon fiber composite depending on the displacement and the initial testing time. It is interested in observing the difference in the logarithmic contact resistivity at the initial state around the maximum stress value. For the untreated case the contact resistivity decreased rapidly, whereas the stress after the maximum decreased smoothly. However, for Zr-treated case the contact resistivity dropped to some degree and then increased again steeply. This might be because of the resistance to be pulled out. The reason for increasing the contact resistivity to the maximum stress value may be related to the minor dimensional change of the carbon fiber itself.

Figure 6 shows SEM photographs of various surfaces of steel and carbon fibers after electro-pulling out testing. The surface of (a) the untreated steel fiber surface exhibits relatively clean and smooth, whereas (b) Zr-treated surface showed the deposited interlayer and (c) the hand-sanded

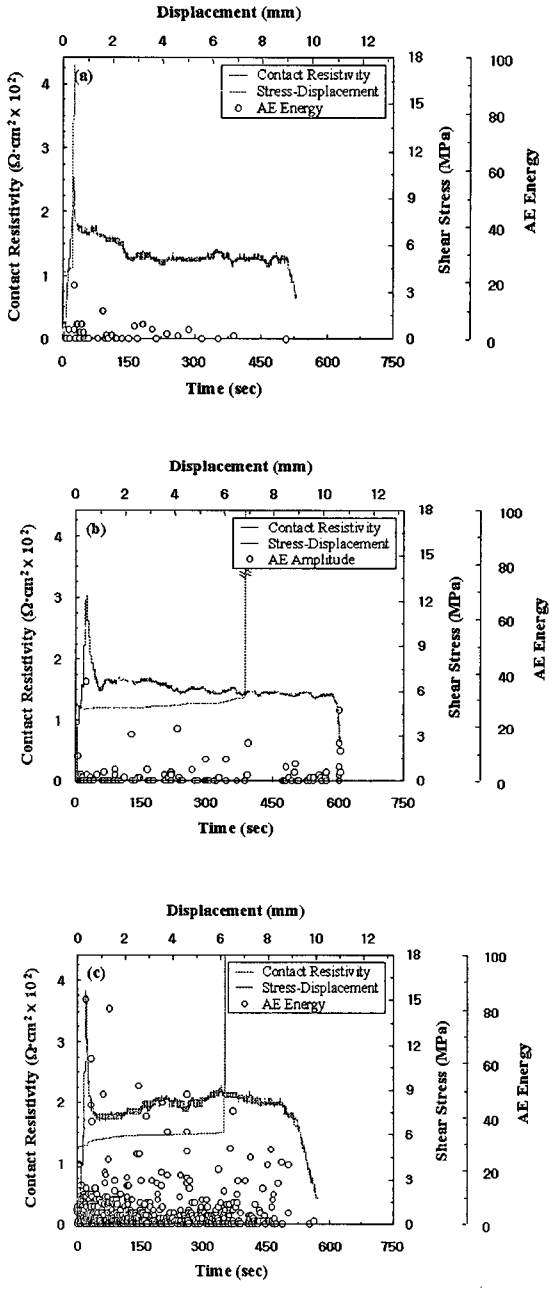

Fig. 3 Comparison of the contact resistivity and AE energy of steel fiber/cement composites during electro-pullout and AE tests: (a) the untreated; (b) Zr-treated; (c) the hand -sanded specimens.

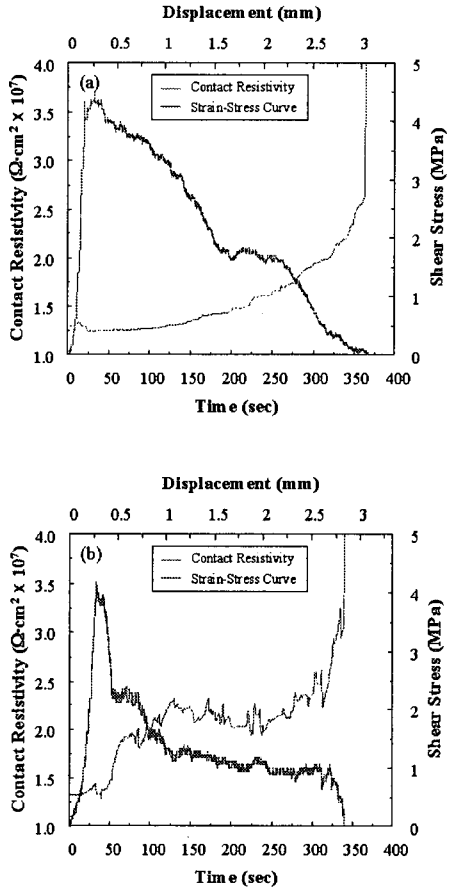

Fig. 4 The contact resistivity and shear stress as a function of total measuring time and displacement for (a) the untreat -ed and (b) Zr-treated carbon fiber/cement during electro-pullout test.

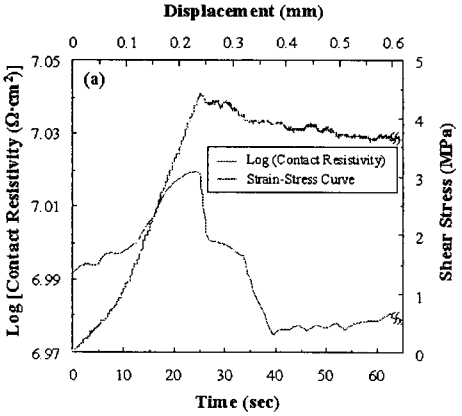

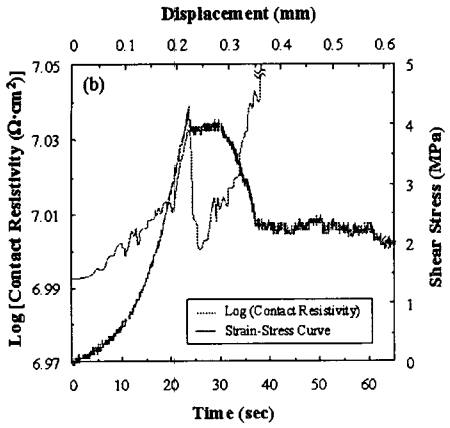

Fig. 5 The contact resistivity and shear stress as a function of initial measuring time and displacement for (a) the untreated and (b) Zr-treated carbon fiber/cement during electro-pullout test.

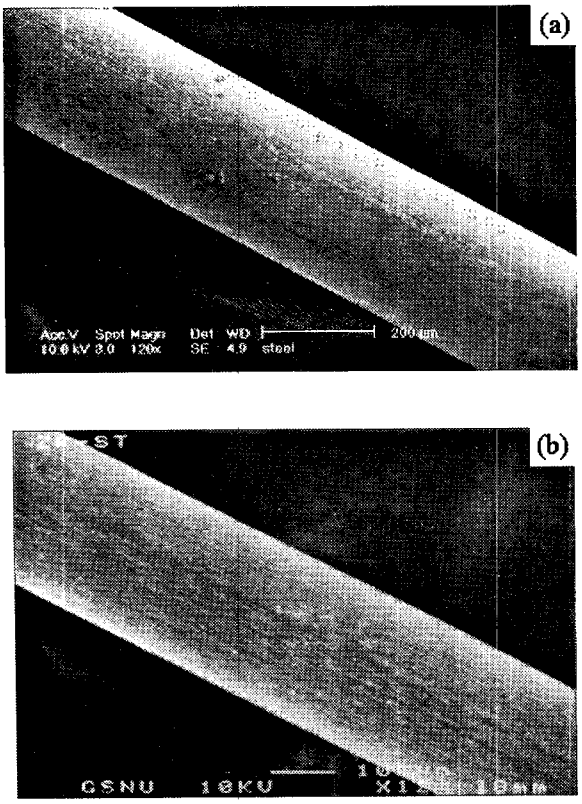

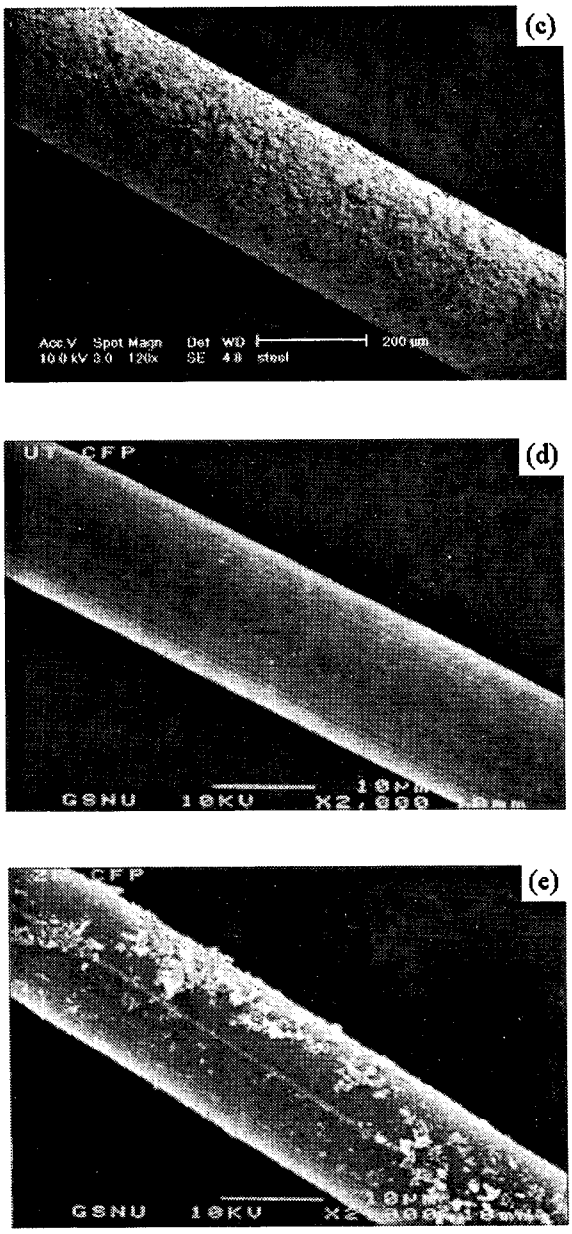

Fig. 6 SEM photographs of typical fiber surfaces after pulling-out: (a) the untreated, (b) Zr-treated, (c) hand-sanded steel fibers; and (d) the untreated, (e) Zr-treated carbon fibers.

composites showed the irregular surface roughness and uniformly attached cement debris, which means the cohesion failure by higher mechanical interlocking.

For carbon fiber case, (d) the cleaning carbon fiber surface showed the neat state after testing, whereas some residual debris was observed on (e) Zr-treated carbon fiber surfaces. The remaining state of debris might be correlated with the interfacial adhesion. Interfacial debonding due to the pullout of carbon fiber might occur in the untreated case without remaining the debris, whereas the frictional failure in Zr-treated carbon fiber composite might result in more debris coming from either cement matrix or interlayer.

3.2 Interfacial Properties and AE Outcomes of Single Glass Fiber/DMC

The main idea of DMC specimen was to allow the composite to undergo the necessary elongation without premature failure of the matrix. Although a fiber breakage can induce the fracture of the adjacent brittle ceramic layer, the crack propagation can be stopped by toughening the supporting epoxy matrix at the second interface, thereby preventing complete fracture of testing specimen. Figure 7 showed the comparison of stress-strain curve and AE amplitude between no-fiber composite and glass fiber/brittle cement/ductile epoxy composite under tensile and compressive tests with AE. AE event number of microfailure exhibited a relatively well-separated group for no-fiber and glass fiber composites for both tensile and compressive tests. The event number of high amplitude in glass fiber composite was observed much more than the case of no-fiber composite. In case of compressive load, many AE event exhibits just until the maximum stress, whereas there are many AE events after yielding point under tensile loading. It might be due to the difference in tensile and compressive failure mechanisms and energies.

Figure 8 exhibits AE amplitude *versus* AE energy for (a) no-fiber and (b) glass fiber DMC specimens under tensile and compressive tests with AE. Comparing to no-fiber specimen case, an AE signal group due to glass fiber break was observed at either high amplitude or energy range under both tensile and compressive tests for glass fiber DMC case. For both no-fiber and glass fiber composites, AE energy under compressive loading was much higher than that of under tensile loading. Comparing to the tensile fracture energy, the compressive fracture energy from brittle cement matrix might be much higher, due to high compressive modulus. It can be because the stress concentrations existed irregularly on the ceramic surface can affect dominantly on the tensile strength. Compared to the tensile testing, the energy loss transferring to AE sensor could be smaller under compressive testing since many overlapped buckling cracks occurred consequently.

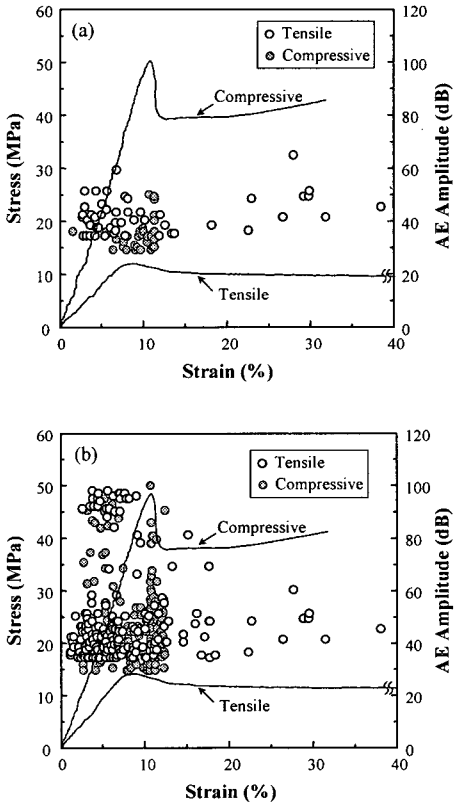

Fig. 7 Stress-strain curve and AE amplitude of single fiber cement composites under tensile and compressive tests: (a) no-fiber composite; (b) glass fiber composite.

Table 3 shows IFSS of glass fiber DMC specimen using tensile fragmentation test. IFSS and average length of matrix crack spacing for glass fiber composite are 15.2 MPa and 467 ㎛, respectively. Crack spacing, 913 ㎛ for glass fiber composite was more than two times wider compared to no-fiber specimen case. It can be reasonably understandable due to the absence of the reinforcing fiber capable to endure transferring stress.

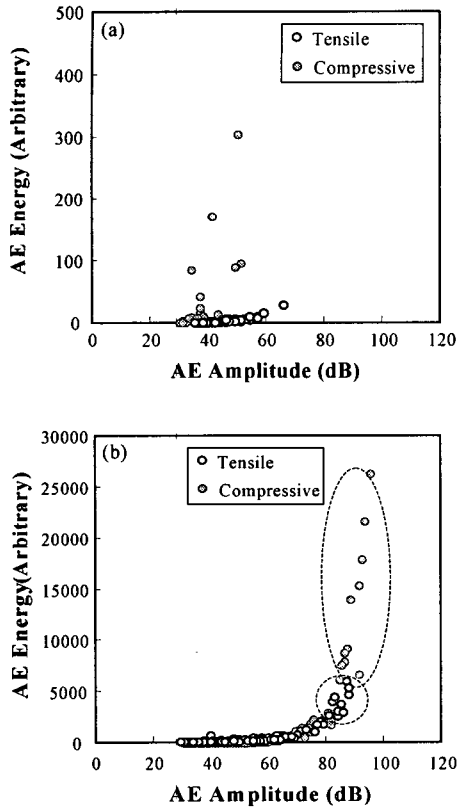

Fig. 8 Comparison of AE amplitude *versus* AE energy in single glass fiber/cement composites under tensile and compressive tests: (a) no-fiber composite; (b) glass fiber composite.

Table 3 IFSS and brittle matrix crack spacing of glass fiber DMC using tensile fragmentation test

Type	σ_{mu} (MPa)	Crack Spacing (μm)	IFSS[1)] (MPa)
Glass Fiber Composite	3.0	467	15.2
No-Fiber Composite	-[2)]	913	-

1) IFSS was calculated using equation (3).
2) Cannot measured

Figure 9 shows photographs of multiple-cement matrix cracks of (a) no-fiber specimen and glass fiber composite under (b) tensile and (c) compressive tests. Less number of diagonal cracks was observed in no-fiber specimen. Crack direction and shape might e dependent upon the existence or the absence of the reinforcing fiber. Vertical microcracks were observed under the tensile test, whereas buckling-shaped and overlapped fracture modes were observed under compressive test. Narrower and buckling cracks being observed under the compressive test was due to the material nature of brittle and strong cement matrix. The reinforcing fiber can endure basically against applying tensile loading, whereas brittle cement matrix can stand against continued compressive loading. Axial compressive load can act on the parallel direction to the fiber axis at the interface. In compressive test, on the other hand, transverse tensile stress can act on the center range intensively in the perpendicular to the fiber axis.

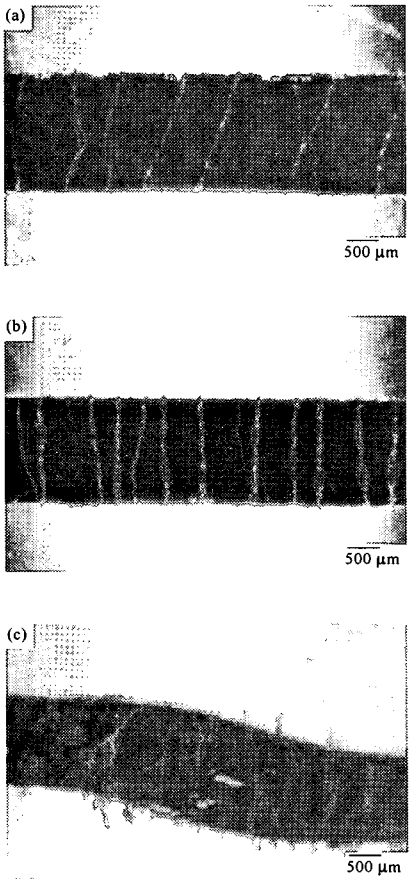

Fig. 9 Typical photographs of the microfailure modes for (a) no -fiber specimen and single glass fiber/cement composites under (b) tensile and (c) compressive loadings.

3.3 AE Waveforms and Their FFT Analysis

Figure 10 shows the typical AE waveforms of (a) the first pullout and (b) the frictional events in the untreated, whereas (c) the first pullout and (d) the frictional events in the hand-sanded steel fiber composites during electro-pullout testing. AE waveforms of the first pullout signal were larger than those of frictional signal in both cases. This might be due to the difference in the microfailure mechanism depending on the surface treatment. AE waveforms of the pullout and frictional signals in the hand-sanded case were larger than those in the untreated case. This trend might be considered that larger AE energy could arise from the retarded interfacial failure energy due to enhanced mechanical interlocking.

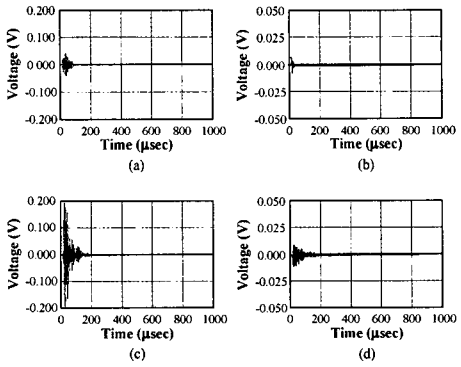

Fig. 10 Comparison of typical AE waveform of the first pull-out and frictional signals depending on the fiber surface trea -tment: (a) the first pull-out and (b) the frictional signal in the untreated composite; (c) the first pull-out and (d) the frictional signal in the hand-sanded steel fiber compo -sites.

Figure 11 shows AE waveforms and their FFT coming from brittle cement matrix in no-fiber specimen under (a) tensile and (b) compressive tests. AE signal from brittle ceramic matrix under compressive test was larger than AE signal of tensile test, which was consistent with the results in Figures 7 and 8. A relatively intensive peak exhibited at 0.3 MHz ranges under tensile test, whereas many peaks exhibited in the wider range from 0.2 to 0.6 MHz under compressive test. Figure 12 shows AE waveforms and their FFT of glass fiber in DMC specimen under (a) tensile and (b) compressive tests. AE signal from brittle ceramic matrix under compressive test was much larger than AE signal under tensile test, which is also consistent with the results in Figures 7 and 8. Under tensile test, characteristic peak coming from fiber breakage appears mainly in the wide range from 0.2 to 0.5 MHz, whereas an intensive peak appeared at 0.3MHz under compressive test. In Figures 11 and 12, FFT trend for no-fiber and glass fiber composites was opposite to each other.

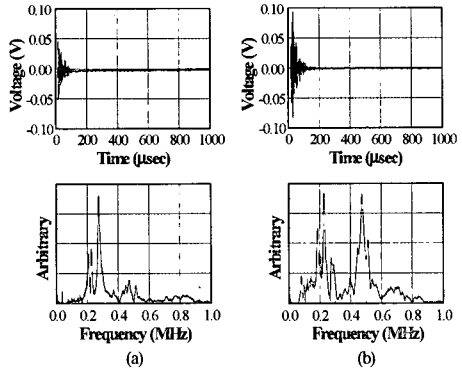

Fig. 11 AE waveforms and their FFT for no-fiber cement composite under (a) tensile and (b) compressive tests.

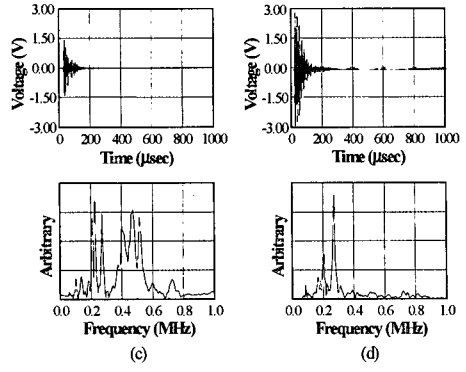

Fig. 12 AE waveforms and their FFT for single glass fiber/cement composite under (a) tensile and (b) compressive tests.

4. CONCLUSIONS

Using electro-pullout technique, the hand-sanded steel fiber cement composite exhibited higher IFSS than either the

untreated or even Zr-treated composites. This might be due to the enhanced mechanical interlocking, compared to hydrogen or covalent bonds coming from possible chemical reactions. During curing process, the contact resistivity decreased rapidly at the initial stage and then showed a level-off for both steel and carbon fiber composites. Comparing to the untreated steel fiber composite, the contact resistivity of either Zr-treated or hand-sanded steel fiber composites increased to the infinity at latter stage. AE waveforms for both the pullout and frictional events in the hand-sanded case are larger than those in the untreated case.

Using DMC, the number of AE signals of hand-sanded steel fiber composite was much more than those of the untreated and Zr-treated cases. More AE signals at high amplitude in glass fiber composite appeared compared to no-fiber composite. AE energy and their AE waveform under compressive loading were much higher and larger than those under tensile loading for both no-fiber and glass fiber composites. This might be due to the ceramic nature showing brittle but enduring well against compressive stress. Vertical cracks for glass fiber composite and rather diagonal cracks for no-fiber specimen exhibits under tensile test. Buckling-sha ped microfailure was observed in glass fiber composite under compressive load. AE waveform from the first pullout signal was larger than that from frictional signal under both tensile and compressive tests. Electro-micromechanical test with AE can be a useful method to evaluate microfailure mechanisms of various conductive fibers/brittle and nontransparent cement matrix composites nondestructively.

ACKNOWLEDGMENT

This study was supported financially by Korea Research Institute of Standards and Science (KRISS).

REFERENCES

1) Okabe, T., Takeda, N., Komotori, J., Shimizu, M., and Curtin, W. A., "A new fracture mechanics model for multiple matrix cracks of SiC fiber reinforced brittle-matrix composites," *Acta Metall.*, Vol. 47, 1999, pp. 4299-4309.

2) Shannag, M., Hansen, W., and Tjiptobroto, P., "Interfacial debonding in fiber reinforced cement-matrix composites," *J. Compos. Mater.*, Vol. 33, 1999, pp. 158-176.

3) Curtin, W. A., "Theory of mechanical properties of ceramic-matrix composites," *J. Am. Ceram. Soc.*, Vol. 74, 1991, pp. 2837-2845.

4) Xia, Z., and Curtin, W. A., "Tough-to-brittle transitions in ceramic-matrix composites with increasing interfacial shear stress," *Acta Mater.*, Vol. 48, 2000, pp. 4879-4892.

5) Curtin, W. A., Ahn, B. K., and Takeda, N., "Modeling brittle and tough stress-strain behavior in unidirectional ceramic matrix composite," *Acta Metall.*, Vol. 46, 1998, pp. 3409-3420.

6) Singh, R. N., "Influence of interfacial shear stress on first-matrix cracking stress in ceramic-matrix composites," *J. Am. Ceram. Soc.*, Vol. 73, 1990, pp. 2930-2937.

7) Sanadi, R., and Piggott, M. R., "Interfacial effects in carbon-epoxies: Part 2. Strength and modulus with short random fibers", *J. Mater. Sci.*, Vol. 20, 1985, pp. 431-437.

8) Pitkethly, M. J., Doble, J. B., and Jacques, P., "Interfacial shear strength evaluation of ceramic-coated carbon fibers," *J. Mater. Sci. Lett.*, Vol. 12, 1993, pp. 1439-1440.

9) Drzal, L. T., "The effect of polymeric matrix mechanical properties on the fiber-matrix interfacial shear strength," *Mater. Sci. Eng.*, Vol. 21, 1990, pp. 289-293.

10) Park, J. M., Shin, W. G., and Yoon, D. J., "A study of interfacial aspects of epoxy-based composites reinforced with dual basalt and SiC fibres by means of the fragmentation and acoustic emission techniques," *Compos. Sci. & Technol.*, Vol. 59, 1999, pp. 355-370.

11) Marshall, D. B., Cox, B. N., and Evans, A. G., "The mechanics of matrix cracking in brittle-matrix fiber composite," *Acta Metall.*, Vol. 31, 1985, pp. 2013-2021.

12) Lee, S. M., and Holguin, S. A., "New single fiber/resin interface test for highly cross-linked resin systems," *J. Adhesion*, Vol. 31, 1990, pp. 91-101.

13) Favre, J. P., and Jacques, D., "Stress transfer by shear in carbon fibre model composites. Part 1. Results of single-fiber fragmentation tests with thermosetting resins," *J. Mater. Sci.*, Vol. 25, 1990, pp. 1373-1380.

14) Lee, S. I., Park, J. M., Shin, D. W., and Yoon, D. J., "Interfacial properties of glass fiber/brittle-ductile dual

matrix composites using micromechanical techniques and acoustic emission," *Polym. Compos.*, Vol. 20, 1999, pp. 19-28.

15) Ageorges, C., Friedrich, K., and Ye, L., "Experiments to relate carbon-fibre surface treatments to composite mechanical properties," *Compos. Sci. & Technol.*, Vol. 59, 1999, pp. 2101-2113.

16) Ageorges, C., Friedrich, K., Schuller, T., and Lauke, B., "Single fiber Broutman test: fiber-matrix interface transverse debonding," *Composite Part A*, Vol. 30, 1999, pp. 1423-1434.

17) Wood, J. R., Wagner, H. D., and Marom, G., "The compressive fragmentation phenomenon: using microcomposites to evaluate thermal stresses, single fibre compressive strengths, Weibull parameters and interfacial shear strengths," *Pro. R. Soc. Lond.*, Vol. A452, 1996, pp. 235-252.

18) Saado, Y., Wood, J. R., and Marom, G., "Thermal shrinkage induced compressive fragmentation in composite materials," *Compos. Interf.*, Vol. 5, 1997, pp. 117-124.

19) Wood, J. R., and Marom, G., "Determining the interfacial shear strength in the presence of transcrystallinity in composites by the single-fiber microcomposite compressive fragmentation test," *App. Compos. Mater.*, Vol. 4, 1997, pp. 197-207.

20) Prasse, T., Michel, F., Mook, G., Schulte, K., and Bauhofer, W., "Electric resistance and acoustic emission during cyclic tensile loading of CFRP laminates," *Proc. ICCM-12*, Paris (France), 1999.

21) Verma, R. K., Kander, R. G., and Hsiao, B. S., "Acoustic emission monitoring of damage using high amplitude gains in carbon fiber reinforced poly(ether ether ketone)," *J. Mater. Sci. Lett.*, Vol. 13, 1994, pp. 438-442.

22) Park, J. M., Chong, E. M., Yoon, D. J., and Lee, J. H., "Interfacial properties of two SiC fiber-reinforced polycarbonate composites using the fragmentation test and acoustic emission," *Polym. Compos.*, Vol. 19, 1998, pp. 747-758.

23) Park, J. M., Kim, Y. M., Kim, K. W., and Yoon, D. J., "Interfacial aspects of electrodeposited carbon fiber-reinforced epoxy composites using monomeric and polymeric coupling agents," *J. Coll. Interf. Sci.*, Vol. 231, 2000, pp. 114-128.

24) Yuse, K., and Bathias, C., "Smart NDT using electrical resistance method for delamination monitoring in CFRP," *Proc. ICCM-12*, Paris (France), 1999.

25) Fu, X., and Chung, D. D. L., "Single-fiber electromechanical pull-out testing and its application to studying the interface between steel fiber and cement," *Compos. Interf.*, Vol. 4, 1997, pp. 197-211.

26) Fu, X., and Chung, D. D. L., "Linear correlation of bond strength and contact the electrical resistivity between steel rebars and concrete," *Cem. Conc. Res.*, Vol. 25, 1995, pp. 1397-1402.

27) Fu, X., and Chung, D. D. L., "Improving the bondstrength between carbon fiber and cement by fiber surface treatment and polymer addition to cement mix," *Cem. Conc. Res.*, Vol. 26, 1996, pp. 1007-1012.

28) Fu, X., and Chung, D. D. L., "Contact the electrical resistivity between cement and carbon fiber: its decrease with increasing bond strength and its increase during pullout," *Cem. Conc. Res.*, Vol. 25, pp. 1391-1396.

29) Wang, X., and Chung, D. D. L., "Residual stress in carbon fiber embedded in epoxy, studied by simultaneous measurement of applied stress and electrical resistance," *Compos. Interf.*, Vol. 5, 1998, pp. 277-281.